Available online at www.sciencedirect.com
ScienceDirect
Progress in Natural Science 19 (2009) 587–594
Progress in Natural Science
www.elsevier.com/locate/pnsc

Cloud microphysical and rainfall responses to zonal perturbations of sea surface temperature: A cloud-resolving modeling study

Xiaopeng Cui [a,*], Xiaofan Li [b], Zhiping Zong [c]

[a] *Laboratory of Cloud-Precipitation Physics and Severe Storms (LACS), Institute of Atmospheric Physics, Chinese Academy of Sciences, Beijing 100029, China*
[b] *Joint Center for Satellite Data Assimilation and NOAA/NESDIS/Office of Research and Applications, Camp Springs, MD, USA*
[c] *National Meteorological Center, China Meteorological Administration, Beijing 100081, China*

Received 20 April 2008; received in revised form 25 July 2008; accepted 10 August 2008

Abstract

The cloud microphysical and rainfall responses to zonal perturbations of sea surface temperature (SST) are investigated by analyzing the equilibrium simulation data (from day 31–40) obtained from a series of two-dimensional cloud-resolving simulations with a zonal model domain of 768 km. Four experiments imposed by zonal SST perturbations of wavenumbers 1 (SST29Z1), 2 (SST29Z2), 4 (SST29Z4), and 8 (SST29Z8) are compared to the control experiment imposed by zonally uniform SST (SST29). The model domain mean SST is 29 °C, and the two-dimensional cloud-resolving model with a cyclic lateral boundary is also imposed by zero vertical velocity and constant zonal wind. The time and model domain mean surface rain rates in SST29Z1, SST29Z2, and SST29Z8 are about 10% larger than those in SST29, whereas the mean surface rain rates in SST29Z4 and SST29 are similar. The analysis of mean surface rainfall budgets shows that local water vapor and hydrometeor changes play important roles in determining the differences and similarities in mean surface rain rate between the perturbation experiments and the control experiment. Both convective and stratiform rain rates are larger in SST29Z1 and SST29Z2 than in SST29 due to the smaller advection of rain from convective regions into raining stratiform regions and the larger vapor condensation rates associated with the larger water vapor convergence over raining stratiform regions in SST29Z1 and SST29Z2. The convective rain rates are larger in SST29Z4 and SST29Z8 than in SST29 because of the larger condensation rates associated with the larger water vapor convergence over convective regions in SST29Z4 and SST29Z8. The stratiform rain rates in SST29Z4 and SST29Z8 are smaller than in SST29 due to the smaller vapor condensation rates and smaller collection rates of cloud water by rain over raining stratiform regions in SST29Z4 and SST29Z8.

Keywords: Cloud microphysical and rainfall responses; Sea surface temperature; Zonal perturbation; Cloud-resolving modeling study

1. Introduction

Sea surface temperature (SST) affects tropical convective development by determining surface evaporation flux as well surface sensible flux [1–5]. Lau et al. [1] compared the experiments with the same large-scale forcing but different SSTs and found that the increase in SST induces surface cooling by increasing surface evaporation and produces a 13% increase in surface precipitation. Cui and Li [6] examined the effects of SST variation on surface rainfall with equilibrium cloud-resolving model simulation data with zero vertical velocity and found that the increase in SST from 29 °C to 31 °C caused 19% increase in surface rain rate.

SST is largely affected by clouds and precipitation through surface heat and freshwater fluxes. Thus, SST shows multi-time and spatial-scale distributions. Cui and

* Corresponding author. Tel.: +86 10 82995105; fax: +86 10 82995308.
E-mail address: xpcui@mail.iap.ac.cn (X. Cui).

1002-0071/$ - see front matter © 2008 National Natural Science Foundation of China and Chinese Academy of Sciences. Published by Elsevier Limited and Science in China Press. All rights reserved.
doi:10.1016/j.pnsc.2008.08.003

Gao [7] studied the effects of zonal perturbations of SST on tropical equilibrium states by comparing four experiments with zonal SST perturbations of wavenumbers 1, 2, 4, and 8 to a control experiment with zonally uniform SST. They found that the experiments with zonal SST perturbations of wavenumbers 1 and 2 produce warmer equilibrium states, whereas the experiments with zonal SST perturbations of wavenumbers 3 and 4 generate colder equilibrium states than the control experiment does. In this study, the cloud microphysical and precipitation responses to zonal perturbations of SST are examined by using the equilibrium simulation data from Cui and Gao [7]. In the next section, the model and experiments are briefly described. The rainfall and cloud microphysical responses to zonally perturbed SST are discussed in Sections 2 and 3, respectively. The summary is given in Section 4.

2. Model and experimental design

The data analyzed in this study were the equilibrium simulations from Cui and Gao [7]. The model was forced by the zonally uniform zero vertical velocity and a zonal wind of $4\ \mathrm{m\ s^{-1}}$. The zonally uniform SST of 29 °C and zonal wavenumbers 1, 2, 4, and 8 with the zonal scale of 768, 384, 192, and 96 km were imposed in experiments SST29, SST29Z1, SST29Z2, SST29Z4, and SST29Z8, respectively. The difference between maximum and minimum SST in the model domain was 1 °C, and the zonal-mean SST was 29 °C in five experiments. The vertical profiles of temperature and specific humidity averaged over the Intensive Flux Array (IFA) during TOGA COARE at 0400 LST 18 December 1992 [8] were used as the initial conditions. The model was integrated for 40.5 days for all five experiments. The equilibrium data were from day 31 to 40. The cloud-resolving model was originally developed by Soong and Ogura [9], Soong and Tao [10], and Tao and Simpson [11] and was further modified by Li et al. [12]. The model with cyclic lateral boundaries includes two prognostic equations for perturbation zonal wind and vertical velocity, two prognostic equations of potential temperature and specific humidity, five prognostic equations for the mixing ratios of cloud water (small cloud droplets), raindrop, cloud ice (small ice crystals), snow (density $0.1\ \mathrm{g\ cm^{-3}}$), and graupel (density $0.4\ \mathrm{g\ cm^{-3}}$). The model uses the cloud microphysical parameterization schemes [13–17], and interactive solar [18] and thermal infrared [19,20] radiation parameterization schemes that are updated every 3 min. The model parameters included a horizontal domain of 768 km, a horizontal grid resolution of 1.5 km, 33 vertical levels, and a time step of 12 s. The model has successfully simulated temperature and water vapor profiles, surface fluxes, and surface rainfall during TOGA COARE and tropical equilibrium states under idealized forcing conditions and the simulation data have been used for process studies toward better understanding of tropical cloud microphysical and surface rainfall processes [21].

3. Rainfall responses to zonal perturbation of SST

To analyze rainfall responses to zonal perturbations of SST, the model domain-mean surface rain rates in the five experiments were analyzed. They are $0.130\ \mathrm{mm\ h^{-1}}$ in SST29, $0.142\ \mathrm{mm\ h^{-1}}$ in SST29Z1, $0.147\ \mathrm{mm\ h^{-1}}$ in SST29Z2, $0.132\ \mathrm{mm\ h^{-1}}$ in SST29Z4, and $0.143\ \mathrm{mm\ h^{-1}}$ in SST29Z8 (Table 1). SST29Z1, SST29Z2, and SST29Z8 produced larger model domain mean surface rain rate by about 10% than SST29 did, while SST29Z4 and SST29 generated similar model domain mean surface rain rates. To explain these difference and similarity in the model domain mean surface rain rate between the five experiments, surface rainfall budgets were calculated. Following a similar derivation in Gao et al. [22], Cui and Li [6], and Ping et al. [23], surface rain rate (P_s) can be expressed by

$$P_s = Q_{\mathrm{WVT}} + Q_{\mathrm{WVF}} + Q_{\mathrm{WVE}} + Q_{\mathrm{CM}} \tag{1}$$

$$Q_{\mathrm{WVT}} = -\frac{\partial[q_v]}{\partial t} \tag{1a}$$

$$Q_{\mathrm{WVF}} = -\left[\bar{u}^o \frac{\partial \bar{q}_v}{\partial x}\right] - \left[\frac{\partial(u'q_v')}{\partial x}\right] - \left[\bar{u}^o \frac{\partial q_v'}{\partial x}\right] - \left[w' \frac{\partial \bar{q}_v}{\partial z}\right] \tag{1b}$$

$$Q_{\mathrm{WVE}} = E_s, \tag{1c}$$

$$Q_{\mathrm{CM}} = -\frac{\partial[q_5]}{\partial t} - \left[u \frac{\partial q_5}{\partial x}\right] - \left[w \frac{\partial q_5}{\partial z}\right] \tag{1d}$$

where Q_{WVT} is the local vapor change, Q_{WVF} is vapor convergence, Q_{WVE} is the surface evaporation (E_s) rate; Q_{CM} is the sum of local hydrometeor change and hydrometeor convergence; u and w are zonal and vertical air wind components, respectively; $q_5 = q_c + q_r + q_i + q_s + q_g$, q_c, q_r, q_i, q_s, q_g are the mixing ratios of cloud water, raindrops, cloud ice, snow, and graupel, respectively; a prime denotes a perturbation from the zonal mean; and the symbol "o" is an imposed forcing.

Since the model uses a cyclic lateral boundary, the model domain mean vapor convergence is zero. The model domain mean surface evaporation rates are $0.134\ \mathrm{mm\ h^{-1}}$ in SST29, $0.129\ \mathrm{mm\ h^{-1}}$ in SST29Z1, $0.130\ \mathrm{mm\ h^{-1}}$ in SST29Z2, $0.129\ \mathrm{mm\ h^{-1}}$ in SST29Z4, and $0.137\ \mathrm{mm\ h^{-1}}$ in SST29Z8 (Table 1). The surface evaporation rate is larger in SST29Z8 than in SST29, which partly explains the larger surface rain rate in SST29Z8. Although the surface evaporation rates account for the model domain mean surface rain rates, they cannot explain the differences in the surface rain rate for SST29Z1-SST29, SST29Z2-SST29, and SST29Z4-SST29. The model domain mean local water vapor change rates are $0.0\ \mathrm{mm\ h^{-1}}$ in SST29, $0.009\ \mathrm{mm\ h^{-1}}$ in SST29Z1, $0.013\ \mathrm{mm\ h^{-1}}$ in SST29Z2, $0.007\ \mathrm{mm\ h^{-1}}$ in SST29Z4, and $0.004\ \mathrm{mm\ h^{-1}}$ in SST29Z8, whereas the model domain mean local hydrometeor change rates are $-0.005\ \mathrm{mm\ h^{-1}}$ in SST29, $0.003\ \mathrm{mm\ h^{-1}}$ in SST29Z1, $0.004\ \mathrm{mm\ h^{-1}}$ in SST29Z2, $-0.004\ \mathrm{mm\ h^{-1}}$ in SST29Z4, and $0.002\ \mathrm{mm\ h^{-1}}$ in SST29Z8. The local atmospheric drying and local hydrometeor loss in SST29Z1 and SST29Z2 and the local hydrometeor gain in SST29 deter-

Table 1
Fractional cloud coverage (%), P_s, Q_{WVT}, Q_{WVF}, Q_{WVE}, and Q_{CM} (mm h^{-1}) over clear-sky regions, raining stratiform regions, convective regions, and non-raining stratiform regions averaged from days 31–40.

	Clear-sky regions	Raining stratiform regions	Convective regions	Non-raining stratiform regions	Model domain mean
SST29					
Fractional coverage	40.7	5.8	4.2	50.1	100
P_s	0.000	0.056	0.074	0.000	0.130
Q_{WVT}	0.013	0.019	−0.011	−0.021	0.000
Q_{WVF}	−0.088	0.007	0.116	−0.034	0.000
Q_{WVE}	0.075	0.004	0.002	0.053	0.134
Q_{CM}	0.000	0.025	−0.033	0.002	−0.005
SST29Z1					
Fractional coverage	39.4	5.2	3.3	51.9	100
P_s	0.000	0.061	0.081	0.000	0.142
Q_{WVT}	0.0016	0.015	−0.008	0.015	0.009
Q_{WVF}	−0.084	0.021	0.105	−0.041	0.000
Q_{WVE}	0.068	0.004	0.003	0.055	0.129
Q_{CM}	0.000	0.020	−0.018	0.002	0.003
SST29Z2					
Fractional coverage	44.2	5.3	3.3	47.0	100
P_s	0.000	0.060	0.087	0.000	0.147
Q_{WVT}	0.019	0.010	−0.006	−0.010	0.013
Q_{WVF}	−0.096	0.026	0.106	−0.036	0.000
Q_{WVE}	0.077	0.004	0.002	0.047	0.130
Q_{CM}	0.000	0.020	−0.015	−0.001	0.004
SST29Z4					
Fractional coverage	45.3	5.3	2.9	47.9	100
P_s	0.000	0.048	0.084	0.000	0.132
Q_{WVT}	0.019	0.018	−0.012	−0.017	0.007
Q_{WVF}	−0.093	0.004	0.129	−0.040	0.000
Q_{WVE}	0.074	0.003	0.002	0.049	0.129
Q_{CM}	0.000	0.023	−0.035	0.007	−0.004
SST29Z8					
Fractional coverage	42.4	5.1	3.3	47.0	100
P_s	0.000	0.051	0.092	0.000	0.143
Q_{WVT}	0.018	0.019	−0.009	−0.024	0.004
Q_{WVF}	−0.093	−0.006	0.136	−0.037	0.000
Q_{WVE}	0.075	0.005	0.003	0.055	0.137
Q_{CM}	0.000	0.033	−0.038	−0.001	0.002

mine the positive difference in the mean surface rain rate for SST29Z1-SST29 and SST29Z2-SST29. Since the local hydrometeor gain rates are similar in SST29Z4 and SST29, the sum of local atmospheric drying rate and surface evaporation rate in SST29Z4 is similar to that of surface evaporation rate in SST29. In addition to the surface evaporation process, the local atmospheric drying and local hydrometeor loss also contribute to larger surface rain rate in SST29Z8 than in SST29.

To further examine convective and stratiform rainfall responses to zonally perturbed SST, the partitioning method developed by Tao et al. [24] and modified by Sui et al. [25] was applied to each grid point to determine the area type (clear sky, raining stratiform, convective, or non-raining stratiform) and the summations of grid points, P_s, Q_{WVT}, Q_{WVF}, Q_{WVE}, and Q_{CM} are taken and divided by the total zonal gird points (512) and the length of hourly data (240). The fractional coverage of convective regions in perturbation experiments is 21–31% smaller than that in the control experiment, whereas the fractional coverage of raining stratiform regions in perturbation experiments is 9–12% smaller than that in the control experiment.

The positive differences in both convective (0.007 mm h^{-1}) and stratiform (0.005 mm h^{-1}) rain rate for SST29Z1-SST29 account for the positive difference in the model domain mean surface rain rate (Table 1). The positive difference in convective rain rate for SST29Z2-SST29 (0.013 mm h^{-1}) and SST29Z8-SST29 (0.018 mm h^{-1}) is responsible for the positive differences in the model domain mean surface rain rate. The positive difference in convective rain rate for SST29Z4-SST29 (0.010 mm h^{-1}) is mainly canceled out by the negative difference in stratiform rain rate (−0.008 mm h^{-1}).

The positive difference in Q_{CM} (0.015 mm h^{-1}) for SST29Z1-SST29 over convective regions mainly causes the positive difference in convective rain rate, since the vapor convergence rate over convective regions is smaller in SST29Z1 (0.105 mm h^{-1}) than in SST29 (0.116 mm h^{-1}) due to the fact that the fractional coverage of convective clouds is smaller in SST29Z1 (3.3%) than in SST29 (4.2%).

The positive difference in Q_{WVF} (0.014 mm h^{-1}) for SST29Z1-SST29 over stratiform regions leads to the positive difference in stratiform rain rate. The positive difference in Q_{CM} (0.018 mm h^{-1}) for SST29Z2-SST29 over convective regions is mainly responsible for the positive difference in convective rain rate. The positive difference in Q_{WVF} (0.013 mm h^{-1}) for SST29Z4-SST29 over convective regions leads to the positive difference in convective rain rate, whereas the negative difference in Q_{WVF} (−0.003 mm h^{-1}) and Q_{CM} (−0.002 mm h^{-1}) for SST29Z4-SST29 over stratiform regions leads to the negative difference in stratiform rain rate. The positive difference in Q_{WVF} (0.020 mm h^{-1}) for SST29Z8-SST29 over convective regions leads to the positive difference in convective rain rate. The positive difference in Q_{WVF} for SST29Z8-SST29 is mainly compensated by the negative difference in Q_{WVF} over stratiform regions (−0.013 mm h^{-1}) and over clear sky regions (−0.005 mm h^{-1}). The negative difference in Q_{WVF} over clear sky regions is nearly balanced by the positive difference in Q_{WVT} (0.005 mm h^{-1}).

4. Cloud microphysical responses to zonal perturbation of SST

To examine the cloud microphysical processes (see Table 2) responsible for development of convective and stratiform rainfall, the cloud microphysical budgets are calculated by averaging equilibrium data over convective (Fig. 1) and stratiform (Fig. 2) regions for all experiments. All five experiments showed that the water hydrometeor microphysical processes are dominant in convective rainfall development, in which the vapor condensation (P_{CND}) leads to the collection of cloud water by rain (P_{RACW}) that causes rain gain (*Sqr*) and surface rainfall (P_s). The melting rates of precipitation ice ($P_{SMLT} + P_{GMLT}$) are at least one order of magnitude smaller than those of P_{RACW}. Over raining stratifrom regions, the melting rates of precipitation ice are about three fifth of the collection rates of cloud water by rain although the vapor deposition rates ($P_{DEP} + P_{SDEP} + P_{GDEP}$) are about one-third of the vapor condensation rates. This suggests the importance of both water and ice hydrometeor microphysical processes in stratiform rainfall development in all five experiments. The microphysics-produced rain rate (*Sqr*) and surface rain rate (P_s) could be different, which could be explained by exchange between convective and stratiform rainfall.

The rates of P_{CND}, P_{RACW}, and *Sqr* are smaller in SST29Z1 (Fig. 1(b)) than in SST29 (Fig. 1(a)), whereas P_s in SST29Z1 is larger. Thus, the convective rain rate is larger in SST29Z1 than in SST29 due to the fact that the advection of rain from convective regions to stratiform regions is smaller in SST29Z1 than in SST29. The rates of P_{CND}, P_{RACW}, and *Sqr* in SST29Z2 and SST29 are similar. The convective rain rate is larger in SST29Z2 (Fig. 1(c)) than in SST29 because the microphysics-produced rainfall accounts for the surface rainfall in SST29Z2, whereas it is advected from convective regions to stratiform regions in SST29. The vapor condensation rate over convective regions is larger in SST29Z4 (Fig. 1(d)) and SST29Z8 (Fig. 1(e)) than in SST29, which leads to larger collection rates of cloud water by rain in SST29Z4 and SST29Z8. As a result, the microphysics-produced rainfall over convective regions and surface convective rainfall are larger in SST29Z4 and SST29Z8 than in SST29.

The vapor condensation rate over raining stratiform regions is larger in SST29Z1 (Fig. 2(b)) than in SST29 (Fig. 2(a)), which causes a larger collection rate of cloud water by rain and a larger microphysics-produced rain rate

Table 2
List of microphysical processes and their parameterization schemes.

Notation	Description	Scheme
P_{REVP}	Growth of vapor by evaporation of raindrops	RH83
P_{CND}	Growth of cloud water by the condensation of supersaturated vapor	TSM
P_{GMLT}	Growth of raindrops by melting of graupel	RH84
P_{SMLT}	Growth of raindrops by melting of snow	RH83
P_{RACW}	Growth of raindrops by the collection of cloud water	RH83
P_{RAUT}	Growth of raindrops by the autoconversion of cloud water	LFO
P_{DEP}	Growth of cloud ice by the deposition of supersaturated vapor	TSM
P_{SAUT}	Growth of snow by the conversion of cloud ice	RH83
P_{SACW}	Growth of snow by the accretion of cloud water	RH83
P_{SFI}	Depositional growth of snow from cloud ice	KFLC
P_{SDEP}	Growth of snow by the deposition of vapor	RH83
P_{GACS}	Growth of graupel by the accretion of snow	RH84
P_{GACW}	Growth of graupel by the accretion of cloud water	RH84
P_{WACS}	Growth of graupel by the riming of snow	RH84
P_{GDEP}	Growth of graupel by the deposition of vapor	RH84
*S*qc	$Sqc = P_{CND} - P_{RACW} - P_{RAUT} - P_{GACW} - P_{SACW}$	
*S*qr	$Sqr = P_{RACW} + P_{RAUT} + P_{GACW}(T > T_o) + P_{SMLT} + P_{GMLT} - P_{REVP}$	
*S*qi	$Sqi = P_{DEP} - P_{SFI} - P_{SAUT}$	
*S*qs	$Sqs = P_{SDEP} + P_{SFI} + P_{SAUT} + P_{SACW} - P_{SMLT} - P_{WACS} - P_{GACS}$	
*S*qg	$Sqg = P_{GDEP} + P_{WACS} + P_{GACS} + P_{GACW}(T < T_o) + P_{GMLT}$	

The schemes are from Rutledge and Hobbs (RH83, RH84) [13,25], Lin et al. (LFO) [14], Tao et al. (TSM) [15], and Krueger et al. (KFLC) [16]. T is air temperature and $T_o = 0$ °C.

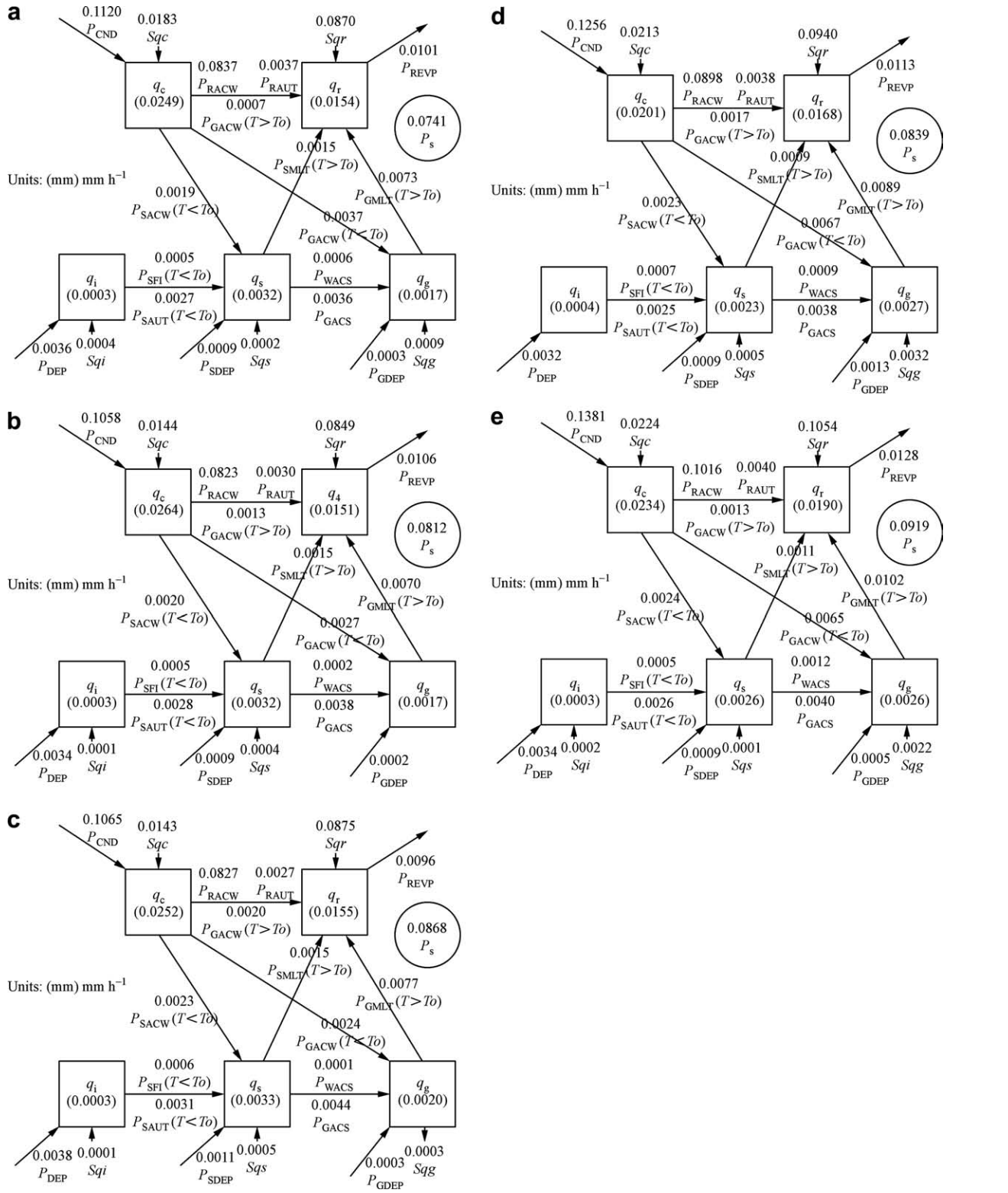

Fig. 1. Cloud microphysics budgets over convective regions averaged from day 31 to day 40 in (a) SST29, (b) SST29Z1, (c) SST29Z2, (d) SST29Z4, and (e) SST29Z8. Units for cloud hydrometeors and conversions are mm and mm h^{-1}, respectively.

in SST29Z1. As a result, surface stratiform rain rate is larger in SST29Z1 than in SST29. The collection rates of cloud water by rain over raining stratiform regions are similar in SST29Z2 (Fig. 2(c)) and SST29 although the vapor condensation rate is larger in SST29Z2 than in SST29. The microphysics-produced rain rate over raining stratiform regions is larger in SST29Z2 than in SST29 because the evaporation rate of rain is smaller in SST29Z2. The larger

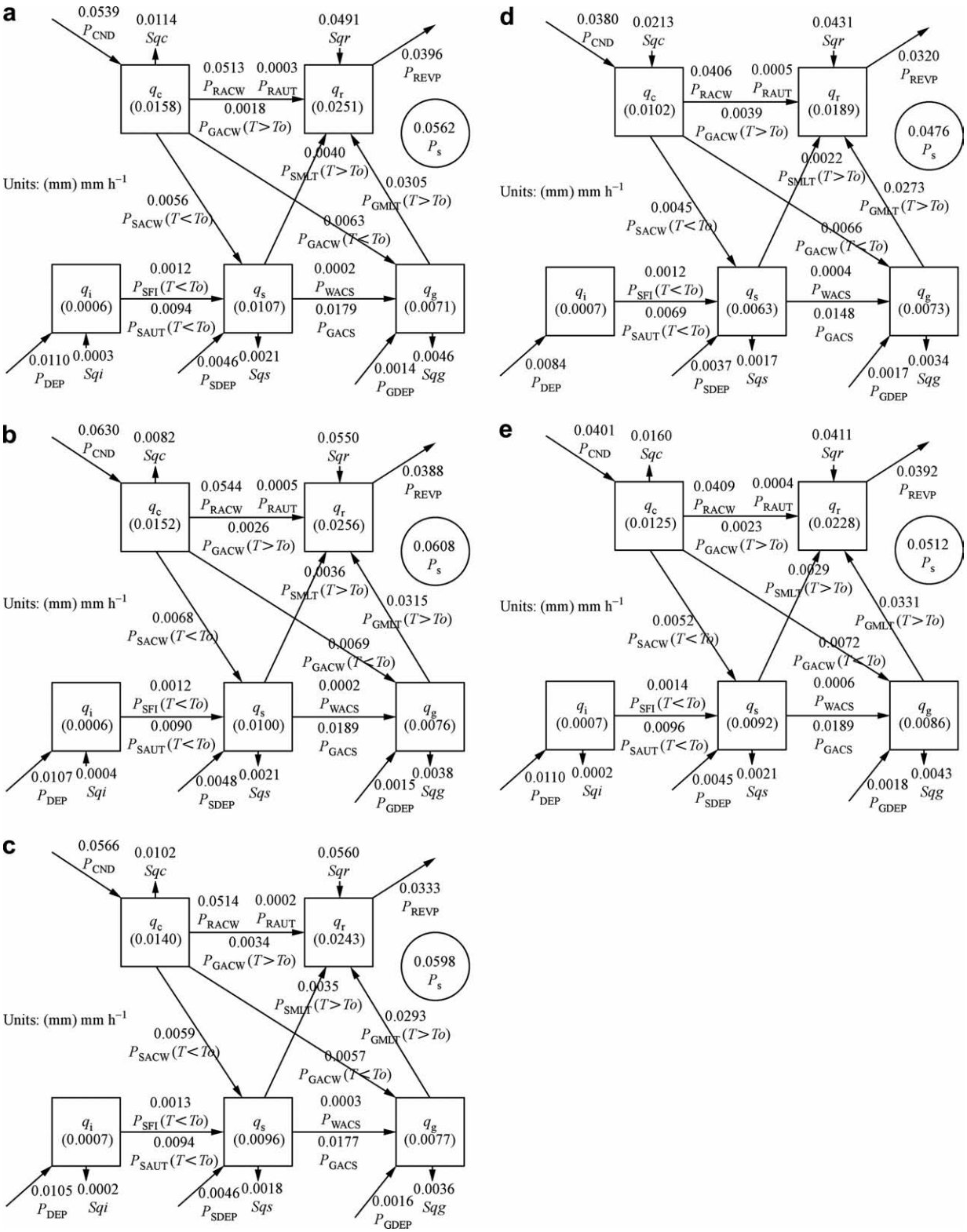

Fig. 2. As in Fig. 1 except over raining stratiform regions.

microphysics-produced rain rate accounts for the surface stratiform rain rate in SST29Z2, compared to SST29. The vapor condensation rate over raining stratiform regions is smaller in SST29Z4 (Fig. 2(d)) and SST29Z8 (Fig. 2(e)) than in SST29, which causes smaller collection rates of cloud water by rain and smaller microphysics-produced rain rates in SST29Z4 and SST29Z8. Thus, the smaller microphysics-produced rain rates determine the smaller

surface stratiform rain rates in SST29Z4 and SST29Z8 than in SST29.

5. Conclusion

The cloud microphysical and rainfall responses to zonal perturbations of sea surface temperature (SST) on tropical equilibrium states are investigated by analyzing the equilibrium simulation data from Cui and Gao [7]. The experiments (SST29Z1, SST29Z2, SST29Z4, and SST29Z8) with zonally varied SST with zonal wavenumbers 1, 2, 4, and 8 (zonal scales of 768, 384, 192, and 96 km) are compared to the control experiment with zonally uniform SST (SST29). The zonal-mean SST in all five experiments is 29 °C. The two-dimensional cloud-resolving model is integrated to the quasi-equilibrium states for 40 days in the framework of zero imposed vertical velocity and constant westerly wind.

The time and model domain mean surface rain rates are about 10% larger in SST29Z1, SST29Z2, and SST29Z8 than in SST29, whereas the mean surface rain rate in SST29Z4 is similar to that in SST29. SST29Z1 and SST19Z2 produce the local atmospheric drying and local hydrometeor loss while SST29 generates the local hydrometeor gain, which explains the positive difference in the mean surface rain rate for SST29Z1-SST29 and SST29Z2-SST29. Similar mean surface rain rates in SST29Z4 and SST29 are due to the facts that SST29Z4 and SST29 produce similar local hydrometeor gain rates and that the surface evaporation rate is slightly smaller in SST29Z4 than in SST29, while the small local atmospheric drying occurs only in SST29Z4. The mean surface rain rate is larger in SST29Z8 than in SST29 because of the local atmospheric drying, local hydrometeor loss, larger surface evaporation rate in SST29Z8 and the local hydrometeor gain in SST29.

Both convective and stratiform rainfalls occupy smaller areas in perturbation experiments than in the control experiment. The convective rain rates are larger in perturbation experiments than in the control experiment, which can be explained by the smaller rain divergence rates in SST29Z1 and SST29Z2 and the larger water vapor convergence rates in SST29Z4 and SST29Z8 over convective regions. The stratiform rain rates are larger in SST29Z1 and SST29Z2 than in SST29 due to the larger water vapor convergence rates over raining stratiform region in SST29Z1 and SST29Z2, whereas they are smaller in SST29Z4 and SST29Z8 because of the smaller water vapor convergence rate in SST29Z4 and water vapor divergence in SST29Z8.

The water hydrometeor microphysical processes are dominant in convective rainfall development, whereas both water and ice hydrometeor microphysical processes are important in stratiform rainfall development. Although the vapor condensation rate and collection rate of cloud water by rain over convective regions are smaller in SST29Z1 and SST29Z2 than in SST29, more advection of convective rain into stratiform regions in SST29Z1 and SST29Z2 is a major process causing the larger convective rain rates in SST29Z1 and SST29Z2 than in SST29. Unlike SST29Z1 and SST29Z2, the larger vapor condensation and collection rates over convective regions in SST29Z4 and SST29Z8 are mainly responsible for the larger convective rain rates, compared to SST29. The larger collection rate and smaller evaporation rate of rain over raining stratiform regions largely account for the larger stratiform rain rate in SST29Z1 and SST29Z2, respectively, than in SST29. The smaller collection rates over raining stratiform regions are mainly responsible for the smaller stratiform rain rates in SST29Z4 and SST29Z8 than in SST29.

Acknowledgements

This work was supported by the National Basic Research Program of China (Grant No. 2009CB421505), National Natural Sciences Foundation of China (Grant No. 40775036), and the Knowledge Innovation Program of the Chinese Academy of Sciences (IAP07214).

References

[1] Lau KM, Sui CH, Chou MD, et al. An inquiry into the cirrus cloud thermostat effect for tropical sea surface temperature. Geophys Res Lett 1994;21:1157–60.
[2] Wu X, Moncrieff MW. Effects of sea surface temperature and large-scale dynamics on the thermodynamic equilibrium state and convection over the tropical western Pacific. J Geophys Res 1999;104:6093–100.
[3] Grabowski WW, Yano JI, Moncrieff MW. Cloud resolving modeling of tropical circulations driven by large-scale SST gradients. J Atmos Sci 2000;57:2022–39.
[4] Yano JI, Grabowski WW, Moncrieff MW. Mean-state convective circulations over large-scale tropical SST gradients. J Atmos Sci 2002;59:1578–92.
[5] Gao S, Zhou Y, Li X. Effects of diurnal variations on tropical equilibrium states: a two-dimensional cloud-resolving modeling study. J Atmos Sci 2007;64:656–64.
[6] Cui X, Li X. Role of surface evaporation in surface rainfall processes. J Geophys Res 2006;111:D17112. doi:10.1029/2005JD006876.
[7] Cui X, Gao S. Effects of zonal perturbations of sea surface temperature on tropical equilibrium states: a 2D cloud-resolving modeling study. Prog Nat Sci 2008;18:413–9.
[8] Sui CH, Lau KM, Takayabu Y, et al. Diurnal variations in tropical oceanic cumulus ensemble during TOGA COARE. J Atmos Sci 1997;54:639–55.
[9] Soong ST, Ogura Y. Response of tradewind cumuli to large-scale processes. J Atmos Sci 1980;37:2035–50.
[10] Soong ST, Tao WK. Response of deep tropical cumulus clouds to mesoscale processes. J Atmos Sci 1980;37:2016–34.
[11] Tao WK, Simpson J. The Goddard Cumulus Ensemble model. Part I: Model description. Terr Atmos Oceanic Sci 1993;4:35–72.
[12] Li X, Sui CH, Lau KM, et al. Large-scale forcing and cloud-radiation interaction in the tropical deep convective regime. J Atmos Sci 1999;56:3028–42.
[13] Rutledge SA, Hobbs PV. The mesoscale and microscale structure and organization of clouds and precipitation in midlatitude cyclones. Part XII: A diagnostic modeling study of precipitation development in narrow cold-frontal rainbands. J Atmos Sci 1984;41:2949–72.

[14] Rutledge SA, Hobbs PV. The mesoscale and microscale structure and organization of clouds and precipitation in midlatitude cyclones. Part VIII: A model for the "seeder-feeder" process in warm-frontal rainbands. J Atmos Sci 1983;40:1185–206.
[15] Lin YL, Farley RD, Orville HD. Bulk parameterization of the snow field in a cloud model. J Climate Appl Meteor 1983;22:1065–92.
[16] Tao WK, Simpson J, McCumber M. An ice-water saturation adjustment. Mon Wea Rev 1989;117:231–5.
[17] Krueger SK, Fu Q, Liou KN, et al. Improvement of an ice-phase microphysics parameterization for use in numerical simulations of tropical convection. J Appl Meteor 1995;34:281–7.
[18] Chou MD, Suarez MJ, Ho CH, et al. Parameterizations for cloud overlapping and shortwave single scattering properties for use in general circulation and cloud ensemble models. J Atmos Sci 1998;55:201–14.
[19] Chou MD, Kratz DP, Ridgway W. Infrared radiation parameterization in numerical climate models. J Climate 1991;4:424–37.
[20] Chou MD, Suarez MJ. An efficient thermal infrared radiation parameterization for use in general circulation model. NASA Tech Memo 104606 1994;3,85 pp. [Available from NASA/Goddard Space Flight Center, Code 913, Greenbelt, MD 20771].
[21] Gao S, Li X. Cloud-resolving modeling of convective processes. Dordrecht: Springer; 2008, p. 206.
[22] Gao S, Cui X, Zhu Y, et al. Surface rainfall processes as simulated in a cloud resolving model. J Geophys Res 2005;110:D10202. doi:10.1029/2004JD005467.
[23] Ping F, Luo Z, Li X. Microphysical and radiative effects of ice microphysics on tropical equilibrium states: a two-dimensional cloud-resolving modeling study. Mon Wea Rev 2007;135:2794–802.
[24] Tao WK, Simpson J, Sui CH, et al. Heating, moisture, and water budgets of tropical and midlatitude squall lines: comparisons and sensitivity to longwave radiation. J Atmos Sci 1993;50:673–90.
[25] Sui CH, Lau KM, Tao WK, et al. The tropical water and energy cycles in a cumulus ensemble model. Part I: Equilibrium climate. J Atmos Sci 1994;51:711–28.